Future 3D Additive Manufacturing
The 3DMM2O Conference

3D Nano- and Micro-Manufacturing:

Technology and Technical Application

REGISTER NOW!

April 3 – 8, 2022 I Schöntal Monastery, Germany

ADVANCED OPTICAL MATERIALS
www.advopticalmat.de

Actively Tunable Collective Localized Surface Plasmons by Responsive Hydrogel Membrane

*Nestor Gisbert Quilis, Marcel van Dongen, Priyamvada Venugopalan, Daria Kotlarek, Christian Petri, Alberto Moreno Cencerrado, Sorin Stanescu, Jose Luis Toca Herrera, Ulrich Jonas, Martin Möller, Ahmed Mourran, and Jakub Dostalek**

Collective (lattice) localized surface plasmons (cLSP) with actively tunable and extremely narrow spectral characteristics are reported. They are supported by periodic arrays of gold nanoparticles attached to a stimuli-responsive hydrogel membrane, which can on demand swell and collapse to reversibly modulate arrays period and surrounding refractive index. In addition, it features a refractive index-symmetrical geometry that promotes the generation of cLSPs and leads to strong suppression of radiative losses, narrowing the spectral width of the resonance, and increasing of the electromagnetic field intensity. Narrowing of the cLSP spectral band down to 13 nm and its reversible shifting by up to 151 nm is observed in the near infrared part of the spectrum by varying temperature and by solvent exchange for systems with a poly(*N*-isopropylacrylamide)-based hydrogel membrane that is allowed to reversibly swell and collapse in either one or in three dimensions. The reported structures with embedded periodic gold nanoparticle arrays are particularly attractive for biosensing applications as the open hydrogel structure can be efficiently post-modified with functional moieties, such as specific ligands, and since biomolecules can rapidly diffuse through swollen polymer networks.

1. Introduction

Plasmonics provides an efficient means for nanoscale manipulation of light[1] in order to push forward the miniaturization and performance characteristics of a variety of optoelectronic technologies.[2] It utilizes metallic nanostructures that support localized surface plasmons (LSPs) originating from collective electron density oscillations coupled with the associated electromagnetic field. The plasmonic materials rapidly find their applications in thin film optical devices for light harvesting,[3] in photocatalysis,[4] nanophotonic circuits,[5] amplified optical spectroscopy,[6] and sensors of chemical and biological species.[7] Recent advances in nanofabrication technologies allowed for the development of facile tools for the preparation of metallic nanostructures with precisely tailored plasmonic characteristics.[8] However, such properties are typically fixed as, after their preparation, the metallic nanostructures cannot be reconfigured. In order to overcome this limitation, there is pursued a new class of plasmonic materials that can be on-demand actuated and thus opens the door for actively controlled nanoscale manipulation with light.[9] These materials are particularly important for integrated optics components such as modulators,[10] switches,[11] and polarizers[12] as well as in plasmonic high resolution displays,[13] and advanced sensing platforms.[14]

Several strategies have been explored for the reversible actuating of LSPs supported by metallic nanostructures.[15]

N. Gisbert Quilis, Dr. P. Venugopalan, D. Kotlarek, Dr. J. Dostalek
BioSensor Technologies
AIT-Austrian Institute of Technology GmbH
Konrad-Lorenz-Strasse 24, 3430 Tulln, Austria
E-mail: jakub.dostalek@ait.ac.at

M. van Dongen, Prof. M. Möller, Dr. A. Mourran
DWI – Leibniz Institute for Interactive Materials
Forckenbeckstrasse 50, 52056 Aachen, Germany

The ORCID identification number(s) for the author(s) of this article can be found under https://doi.org/10.1002/adom.201900342.

DOI: 10.1002/adom.201900342

Dr. P. Venugopalan
CEST Kompetenzzentrum für elektrochemische Oberflächentechnologie GmbH
TFZ, Wiener Neustadt
Viktor-Kaplan-Strasse 2, 2700 Wiener Neustadt, Austria

Dr. C. Petri, Prof. U. Jonas
Macromolecular Chemistry
Department Chemistry-Biology
University of Siegen
Adolf Reichwein-Strasse 2, Siegen 57076, Germany

Dr. A. Moreno Cencerrado, Prof. J. L. Toca Herrera
Institute for Biophysics
Department of Nanobiotechnology
University of Natural Resources and Life Sciences Vienna (BOKU)
Muthgasse 11, Vienna 1190, Austria

Dr. S. Stanescu
LIG Nanowise Ltd
Williams House
Manchester Science Park
Manchester M15 6SE, UK

In particular, materials capping metallic nanostructures and exhibiting a tunable real part of the refractive index (by an external stimulus such as light,[16] temperature,[17] pH,[18] and electric current[19]) were pursued capitalizing on the sensitivity of LSPs to the optical density of surrounding medium. In addition, simultaneously modulating both the real and the imaginary part of the refractive index was demonstrated to strongly and reversibly shift the LSP excitation wavelength via electrochemical switching.[20] Another approach to actuate LSPs was explored based on the near field coupling between metallic nanoparticles with modulated gap distance[21,22] and by dynamically controlled far-field coupling to LSPs on periodic arrays of aluminum nanoparticles.[23] Chemically synthesized plasmonic nanoparticles were actuated by the pH-responsive polymer brushes[22] and the lithographically prepared aluminum nanoparticles were attached to polydimethylsiloxane elastomer[23] and mechanically stretched to reversibly vary the arrays period enabling tuning the excitation of LSP over the whole visible part of the spectrum. Besides controlling the surrounding environment of plasmonic nanoparticles, also the SPR-active material itself can be actuated as was showed by modulating the concentration of charge carriers in graphene nanostructures leading to strong spectral shifts of the plasmonic resonances in the near and mid infrared part of the spectrum.[24]

The vast majority of the reported actuated plasmonic nanostructures exhibit shifts in the LSPR wavelength that are smaller than the actual spectral width of the resonance, mostly because of employing absorbing materials.[25] Therefore complete switching "off" and "on" of the resonances is not possible, which limits the utilization of active plasmonic materials in the envisaged applications. To decrease the damping of LSPs, periodic arrays of metallic nanoparticles can be embedded in refractive index-symmetric geometry and thus exploit the diffraction coupling between neighboring nanoparticles.[26] Such structures can be designed to support collective (lattice) localized plasmon (cLSPs) with decreased radiative losses, which is manifested as spectrally sharp plasmonic features[27] and is associated with stronger field intensity enhancement[28] compared to regular LSPs. These characteristics make plasmonic nanostructures supporting cLSPs attractive candidates for sensing of molecular species,[29] enhanced optical spectroscopy,[30] light harvesting,[31] and lasing.[32] As refractive index symmetry is required, typically immersion oils are employed to match the refractive index above and below the particle arrays in order to observe the cLSPs on glass or silicon substrates.[33] Only recently the using of low refractive index fluoropolymer layers enabled the excitation of cLSPs in aqueous environments[34] and self-assembled metallic nanoparticle arrays embedded to tethered responsive hydrogel layer and swollen in water were reported for switching of cLSP resonances.[35] The present paper reports on the implementation and strong actuating of cLSPs by using structures that rely on responsive hydrogel materials. A new approach to prepare periodic arrays of gold nanoparticles supported by either free-standing or surface-attached thermo-responsive poly(*N*-isopropylacrylamide)-based (pNIPAAM) hydrogel membrane was developed by using laser interference lithography combined with template stripping. The specific design of the geometry enables active tuning of the cLSP excitation by reversibly changing the refractive index symmetry as well as the lattice periodicity. In addition, the hydrogel materials swollen in aqueous environment provide the refractive index symmetry suitable for plasmonic biosensing applications and superior performance characteristics in refractometric-based surface plasmon resonance biosensors are demonstrated.

2. Results and Discussion

Two types of structures with actuated plasmonic properties were prepared. As **Figure 1** illustrates, these structures comprise gold nanoparticle arrays embedded on the top of surface-attached (A) or free-standing (B) responsive hydrogel membrane. The arrays

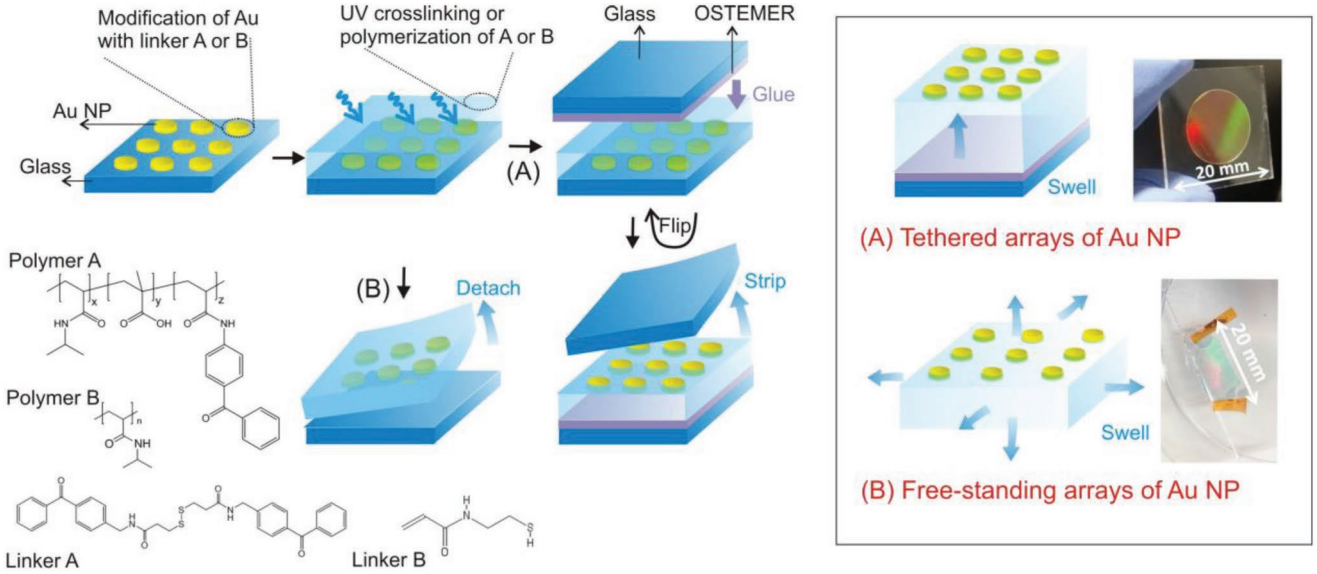

Figure 1. Schematic of the route for the preparation of gold nanoparticles arrays carried by A) tethered and B) free-standing pNIPAAm hydrogel film. The swelling of the structures in one and three dimensions is sketched in the right part together with examples of prepared materials.

of gold nanoparticles were fabricated by the UV laser interference lithography (UV-LIL) on a glass substrate that was modified with an anti-sticking layer. For the preparation of the surface-attached structure (A), the gold nanoparticles were decorated with photoactive benzophenone moieties (linker A). Then, pNIPAAm-based terpolymer with benzophenone groups attached to its chain (polymer A) was deposited on their top with a layer thickness of d_h = 0.28 µm followed by its simultaneous crosslinking and attaching to gold by irradiation with UV light. Finally, the structure was contacted and bonded to another glass substrate with a thin elastic Ostemer layer carrying epoxy groups. After the curing, the structure was stripped yielding the gold nanoparticles arrays supported by a surface-attached pNIPAAm-based terpolymer cushion. The second structure with a free-standing hydrogel membrane (B) utilized arrays of gold nanoparticles that were reacted with *N*,*N*′-bis(acryloyl)cystamine (linker B). On their top, a pNIPAAm layer (polymer B) with a thickness of d_h = 40 µm was in situ synthesized upon UV light irradiation. Contrary to the previous structure, the thicker crosslinked polymer layer with embedded periodic arrays of gold nanoparticles was detached by its swelling in ethanol in order to form a free-standing membrane.

2.1. Morphology of cLSP Arrays

The period Λ and diameter D of the arrays of gold nanoparticles was controlled in the range Λ = 360–560 nm and D = 110–200 nm, respectively, by adjusting the UV-LIL parameters.[36] **Figure 2**a shows an example of the topology of gold nanoparticle arrays prepared on glass substrate prior to the attachment of pNIPAAm-based polymer. The topology was observed by atomic force microscopy (AFM) and it reveals cylindrically shaped gold nanoparticles with a height of about h = 50 nm. As seen in Figure 2b, the height of the structure decreases after the embedding of gold nanoparticles to a pNIPAAm polymer layer in a surface-attached geometry (A). The pNIPAAm polymer networks in such structure swell when brought in contact with water (kept below the local solution critical temperature–LCST), which lifts up the nanoparticle arrays by the formed soft hydrogel cushion exhibiting low Young modulus.[37] Then, the in situ AFM does not capture the presence of gold nanoparticles as indicated by Figure 2c. The measured topology of the surface shows irregular features that can be attributed to the lateral stress-induced buckling of a thin hydrogel film that, due to surface attachment, is allowed to swell only in the direction perpendicular to the surface. Interestingly, the periodic pattern of gold nanoparticles suspended in swollen hydrogel retains its periodic arrangement as observed by the complementary optical measurements of structure B with a high numerical aperture lens, see the inset of Figure 2c. When increasing the temperature above pNIPAAm LCST of T_{LCST} = 32 °C, the hydrogel polymer network collapses, the Young modulus increases, and the AFM performed in water again reveals the periodic arrays of gold nanoparticles as documented by Figure 2d. In this figure, small protrusions with characteristic size of about hundred nanometers can be seen as dark spots in the structure topology. Such domains were observed after the swelling and subsequent drying of similar hydrogel films (without embedded gold nanoparticle arrays) and they were attributed to the effect of "skin barrier" that was reduced by the incorporation of polar methacrylic acid to the polymer backbone (polymer A).[36]

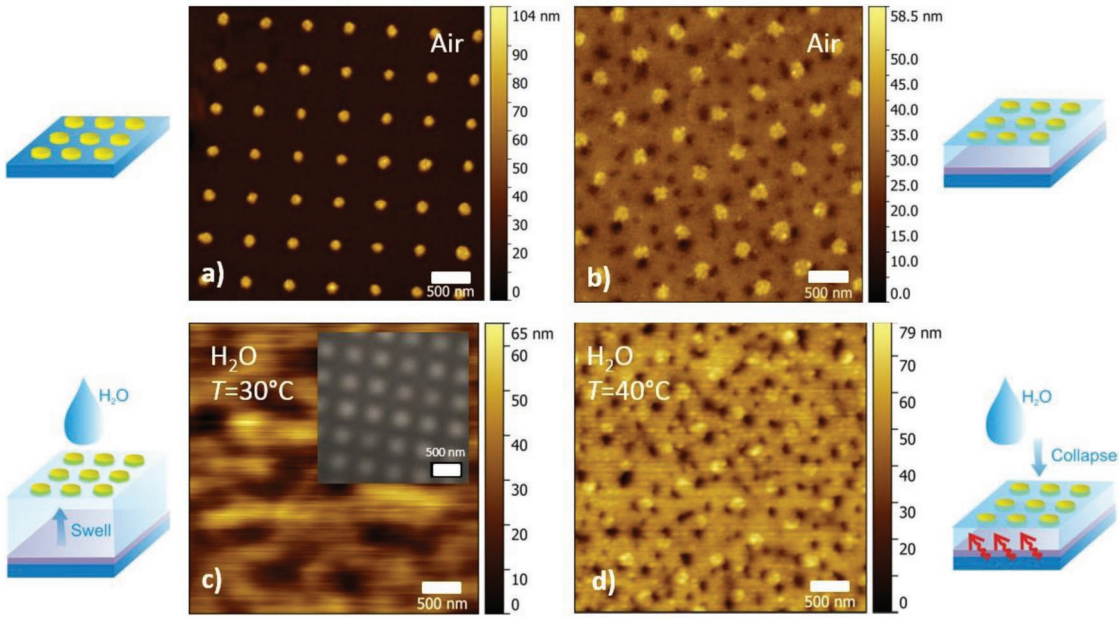

Figure 2. AFM observation of gold particle arrays on a) glass substrate after the UV-LIL fabrication (prepared with Λ = 560 nm, D = 150 nm), b) after their embedding to pNIPAAm-based polymer in a structure A followed by the rinsing with water and drying at a temperature above the pNIPAAm LCST (both images were taken in air). Observation of the tethered structure A in contact with water c) at T = 30 °C in swollen state and d) at T = 40 °C in the collapsed state. The inset in figure (c) represents an optical microscopy image of the swollen free-standing hydrogel film (structure B prepared with Λ = 360 nm, D = 140 nm) in water at room temperature.

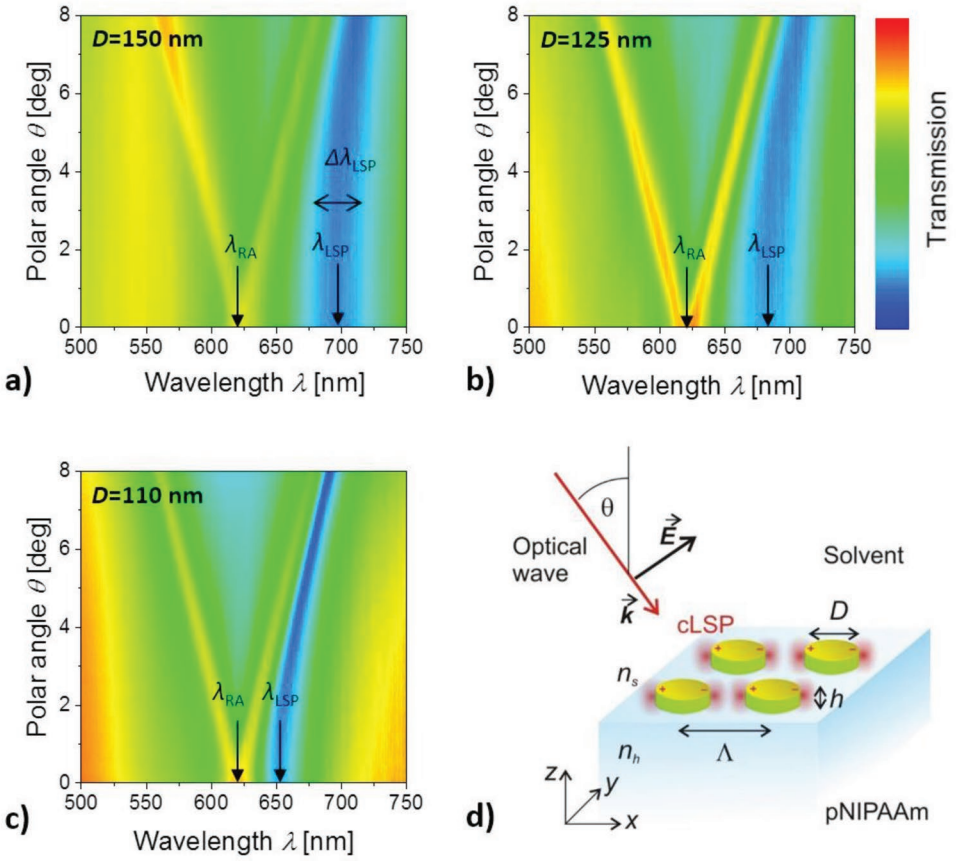

Figure 3. Angular–wavelength transmission spectra measured for the tethered structure A in contact with water at T = 22 °C. The spectra were measured with TE polarization and the diameter of gold nanoparticles was varied as a) D = 150 nm, b) D = 125 nm, and c) D = 110 nm while the period was set to Λ = 460 nm. d) Schematics of the used geometry with arrays of gold nanoparticles that are probed by an incident optical wave.

2.2. Optical Characteristics of cLSP Structures

The changing of temperature below or above T_{LCST} of used thermo-responsive pNIPAAm polymer networks is accompanied by abrupt volume changes. These changes are associated with the polymer density variations, which translate to the modulating of hydrogel refractive index n_h. The surface-attached pNIPAAm layer in its hydrated swollen state ($T < T_{LCST}$) exhibits a low refractive index of $n_h = 1.36$ while in its collapsed state ($T > T_{LCST}$) the refractive index increases to $n_h = 1.46$. These parameters were measured by optical waveguide spectroscopy combined with surface plasmon resonance[38] for the layer used in the geometry A. The measurements revealed that the swelling of the film perpendicular to its surface leads to the increase in its thickness from d_h = 275 nm to about 1 µm (data not shown). In its swollen state, the prepared pNIPAAm hydrogel exhibits a refractive index n_h that is close to that of water n_s = 1.33, which generates nearly symmetrical geometry around the arrays of gold nanoparticles. Such configuration promotes the diffraction coupling of LSPs supported by individual gold nanoparticles and it leads to the establishment of collective (lattice) modes–cLSPs. As investigated before, such modes occur when the spectral position of diffraction Rayleigh anomaly λ_{RA} is in the vicinity to LSP wavelength λ_{LSP}.[39] In order to tune the spectral distance between λ_{LSP} and λ_{RA}, the diameter D of gold nanoparticle arrays was adjusted for a period fixed at Λ = 460 nm. As reported before, varying diameter of arrays of gold nanoparticles from D = 150 to 110 nm leads to a shift of the λ_{LSP} by 50 nm.[36] Therefore, decreasing the diameter D was utilized to push λ_{LSP} closer to the Rayleigh anomaly and thus to generate the cLSP mode. Such behavior is observed in the measured angular–wavelength transmission spectra presented in **Figure 3**. In these data, one can see a characteristic V-shaped feature centered at $\lambda_{RA} = \Lambda n_h \approx 620$ nm, which corresponds to the splitting of λ_{RA} when deviating the incident angle θ. At longer wavelengths, there can be seen a dip associated to the resonant excitation of LSPs that is shifting from 700 to 650 nm when decreasing the diameter D. Importantly, the LSP resonance wavelength λ_{LSP} become angular dispersive and its spectral width $\Delta\lambda_{LSP}$ decreases when decreasing D, which can be attributed to its gradual shifting to the vicinity to λ_{RA} and diffraction coupling of cLSPs. The dispersive cLSPs band is observed for the transversally electric polarization of the incident beam (TE, with the electric field intensity vector parallel to the surface) as illustrated in Figure 3d showing the schematics of the geometry.

2.3. Actuating of cLSPs Arrays

The spectrally narrow resonances associated with the excitation of cLPSs can be actuated by breaking the refractive index

symmetry or by varying the arrays period Λ. The surface-attached structure A is allowed to swell and collapse only in perpendicular direction and thus only changing the refractive index symmetry is possible. The free-standing structure B is allowed to swell and collapse also in the lateral direction and therefore one can take advantage of the combined effect of modulating the arrays period Λ and refractive index n_h. The first approach was tested for the architecture A with Λ = 460 nm and D = 110 nm. As can be seen in **Figure 4**a, the temperature-triggered variations in the refractive index $\Delta n_h \approx 0.10$ induced a reversible shift in the spectral position of cLSP resonance λ_{LSP}. The shift of $\delta\lambda_{LSP}$ = 18.5 nm was measured in the transmission spectrum for the normally incident optical beam $\theta = 0°$. In addition, it illustrates that the perturbation of refractive index symmetry by the increasing of temperature leads to an increase in the spectral width of the resonance from $\Delta\lambda_{LSP}$ = 38 nm in swollen state (cLSPs are excited) to $\Delta\lambda_{LSP}$ = 73 nm when the hydrogel is collapsed (regular LSPs are excited). Similar experiment was carried out for the structure B carrying arrays of gold nanoparticles with Λ = 360 nm and D = 140 nm on the top of free-standing hydrogel membrane. When swollen in water at a temperature below T_{LCST}, the structure expands in lateral direction and the period of arrays increases to about Λ = 525 nm, which is manifested as a shift of the first diffraction order Rayleigh anomaly to λ_{RA} = 700 nm. As Figure 4b shows, the spectral position of the cLSPs is then located at a longer wavelength of λ_{LSP} = 747 nm and exhibits the spectral width $\Delta\lambda_{LSP}$ = 66 nm. This width is wider compared to that for the surface-attached structure (A), which can be attributed to the larger diameter D of used nanoparticles. When increasing the temperature above the NIPAAm T_{LCST}, the spectral position λ_{LSP} shifts opposite compared to the structure A toward shorter wavelength of λ_{LSP} = 686 nm and the spectral width increases to $\Delta\lambda_{LSP}$ = 120 nm. The reason for the blueshift of the resonance is the decreasing of the period Λ below 380 nm due to the shrinking of the structure, which stronger impacts the resonance compared to the increase of refractive index n_h (that redshifts the resonance position). It is important to note that the observed temperature actuating of responsive hydrogel membrane is accompanied with more than one order of magnitude stronger refractive index changes Δn_h compared to that occurring for water in the used temperature range.[33] Interestingly, when incubating the structure in ethanol, both λ_{RA} and λ_{LSP} are redshifted to 820 and 838 nm, respectively, and the spectral width of LSP resonance decreases to λ_{LSP} = 22 nm. This observation can be explained by the fact that ethanol acts as a better solvent than water. Therefore, the period is prolonged to about Λ = 600 nm and refractive index of more swollen hydrogel n_h is closer to that of the solvent n_s. In addition, the refractive index of ethanol n_s is higher than that of water, which further contributes to the red spectral shift. The performed measurements reveal that reproducible reversible shifts of $\delta\lambda_{LSP}$ = 61 nm were obtained by the repeated switching between the collapsed and the swollen state in water through modulating temperature T. Even stronger shifts of $\delta\lambda_{LSP}$ = 151 nm were observed for the changing of solvent between ethanol and water at a temperature above T_{LCST}. It is worth of mentioning that the pNIPAAm-based hydrogel film does not exhibit thermo-responsive behavior in ethanol[40] and thus changing temperature T does significantly affect the cLSP resonance in this solvent. The variations in λ_{LSP} are fully reversible and no changes were observed after more than five cycles of swelling in different solvents and modulated temperature, see Figure 4d.

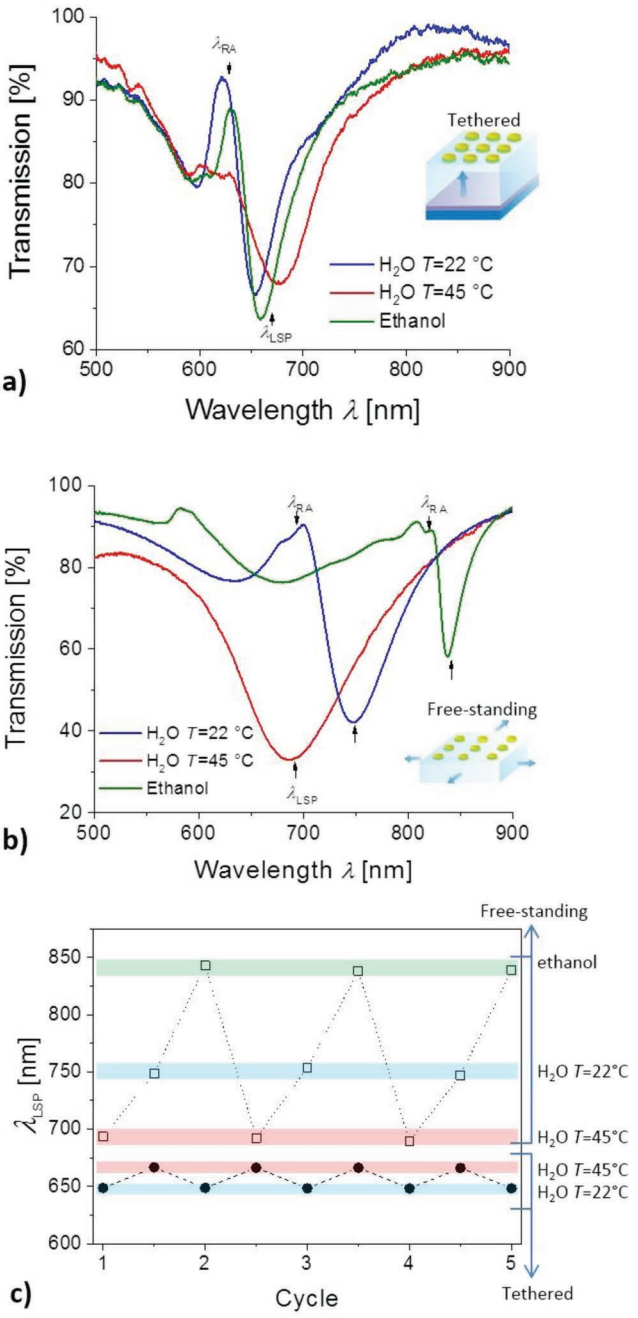

Figure 4. Transmission spectra measured for a) tethered structure (A, prepared with Λ = 460 nm, D = 110 nm) and b) free-standing structure (B, prepared with Λ = 360 nm, D = 140 nm) in contact with water at T = 22 °C (blue curve), T = 45 °C (red curve), and in contact with ethanol (green curve) at room temperature for the normally incident beam $\theta = 0°$. c) Measured changes in the wavelength λ_{LSP} upon series of five cycles of swelling and collapsing in H_2O and in ethanol for tethered (bottom) and free-standing (top).

2.4. Numerical Simulations

Based on the FDTD method, series of transmission spectra and distribution of near field intensity were simulated for the structure B that resembles arrays of gold nanoparticles on the top of the actuated free-standing hydrogel membrane (see Figure 4b). The simulated transmission spectra are presented in **Figure 5** and they were obtained for the geometry describing the collapsed structure in water (I), swollen structure in water (II), and swollen structure in ethanol (III). These data show that the spectral positions of transmission dips λ_{LSP} associated with the resonant coupling to LSPs closely match the experimental values while the spectral widths [$\Delta\lambda_{LSP}$ = 115 nm (I); $\Delta\lambda_{LSP}$ = 34 nm (II); $\Delta\lambda_{LSP}$ = 13 nm (III)] are narrower compared to experimental values [$\Delta\lambda_{LSP}$ = 120 nm; $\Delta\lambda_{LSP}$ = 66 nm; $\Delta\lambda_{LSP}$ = 22 nm, respectively]. These discrepancies can be attributed to slight variations in the morphology of the prepared gold nanoparticle arrays over the measured surface area.[36] The near field simulations were carried out for the wavelengths λ_{LSP} corresponding to the resonant excitation of LSPs. For the nonsymmetrical configuration I (when regular LSPs are excited) the field intensity enhancement peaks at the gold nanoparticle wall and decays when increasing the distance from the wall of gold nanoparticle. When normalized with the electric intensity of the incident beam, the field intensity enhancement at the nanoparticle walls yields $|E/E_0|^2 = 100$. For the geometry resembling the nanoparticle arrays on hydrogel cushion swollen in water II, the establishing of cLSPs leads to stronger maximum field intensity enhancement of $|E/E_0|^2 = 375$. Moreover, the increasing of the period Λ by swelling in ethanol (III) shifts the resonance closer to the Rayleigh anomaly λ_{RA} and the field intensity enhancement reaches a value as high as $|E/E_0|^2 = 814$. The confined LSP field intensity probes to the distance of d = 14 nm (field intensity drops to half) for the geometry I and the mode supported at longer wavelengths on the structure III exhibits more delocalized field intensity profile probing up to the distance of 17 nm, see Figure 5c.

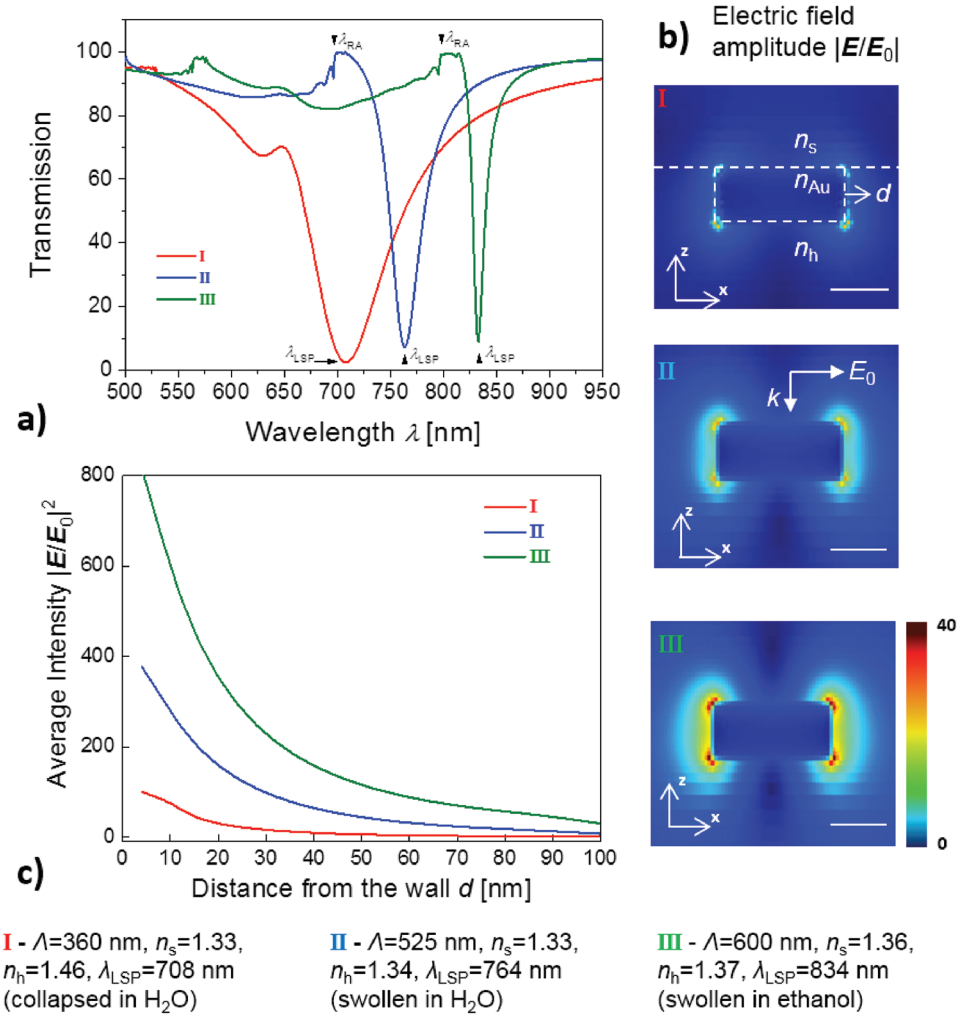

Figure 5. a) Simulated transmission spectra, b) spatial distribution electric field amplitude, and c) cross-section of the electric field intensity averaged over walls of gold nanoparticle arrays (with D = 140 nm) for the geometry experimentally determined for the free-standing structure B observed in Figure 4. The parameters used to represent the collapsed state in water (I, red), swollen state in water (II, blue), and swollen state ethanol (III, green) are stated at the bottom of the figure.

2.5. Refractometric Sensing Measurements

The examined surface-attached structure A was prepared by using a pNIPAAm-based terpolymer with incorporated methacrylic acid that can be post-modified with biomolecules in order to serve as a large capacity binding matrix in affinity biosensors. This functionality was already demonstrated in a variety of assays based on refractometric surface plasmon resonance[38,41] and surface plasmon-enhanced fluorescence[42] with amine coupling of ligand biomolecules[43] that are specific to target analyte. The probing of target analyte biomolecules that diffuse through hydrogel open polymer networks and become affinity captured can be performed by the enhanced intensity of cLSP field. This approach holds potential for improved sensitivity compared to classical LSP resonance sensors due to the narrower resonance of cLSPs resonances and thus improved figure of merit. The figure of merit (FOM) can be defined as a ratio of refractive index sensitivity of LSP resonant wavelength $\delta\lambda_{LSP}/\delta n_s$ and the width of the resonance $\Delta\lambda_{LSP}$.

First, we investigated the dependence of the width of the spectral band $\Delta\lambda_{LSP,}$ on the angle of incidence θ for the structure A with $\Lambda = 460$, $D = 110$ nm, and swollen hydrogel cushion. As seen in Figure 3, the overlapping of the Rayleigh anomaly λ_{RA} with λ_{LSP} can be adjusted by varying θ, which thus provides an additional facile handle to control the cLSPs damping. The measured transmission spectra presented in **Figure 6**a show that increasing θ leads to the splitting of the cLSP resonance and its long wavelength branch is redshifted and its spectral width $\Delta\lambda_{LSP}$ is gradually decreased due to the approaching of λ_{RA} to λ_{LSP}. These observations are summarized in Figure 6b and show that the increase of the angle of incidence θ from 0° to 8° shifts λ_{LSP} from 655 to 695 nm and is accompanied with a decrease of the full width in the half minimum of the resonance $\Delta\lambda_{LSP}$ from 38 to 13 nm.

Second, we observed the refractive index sensitivity of prepared structure $\delta\lambda_{LSP}/\delta n_s$ for the same structure. Aqueous solutions spiked with sucrose were prepared to control the refractive index n_s between 1.330 and 1.339 refractive index units (RIU). These solutions were sequentially flowed over the plasmonic structure surface and transmission spectra were measured for the angle of incidence $\theta = 8°$. As can be seen in **Figure 7**a, increasing of the refractive index n_s is accompanied with a redshift of the cLSP wavelength λ_{LSP} and the refractive index sensitivity of $\delta\lambda_{LSP}/\delta n_s = 372$ nm/RIU was measured. As summarized in **Table 1** for other investigated geometries, this sensitivity is higher compared to that measured for the collapsed hydrogel cushion as the swollen polymer networks supporting the nanoparticle arrays enables accessing of the whole volume probed by cLSPs for sensing. In a nutshell, the using of hydrogel membrane carrying arrays of gold nanoparticle allows tightly overlapping the λ_{LSP} and λ_{RA} leading to a figure of merit reaching values as high as FOM = 29 in aqueous environment. In addition, the hydrophillic hydrogel networks can be post modified with capture proteins as was demonstrated for covalent attaching of IgG antibodies, which has been manifested as a shift of 6 nm in the data presented in Figure 7b.

The developed material provides FOM above the values reported before for other plasmonic nanoparticle arrays supporting cLSPs on quartz substrate with refractive index

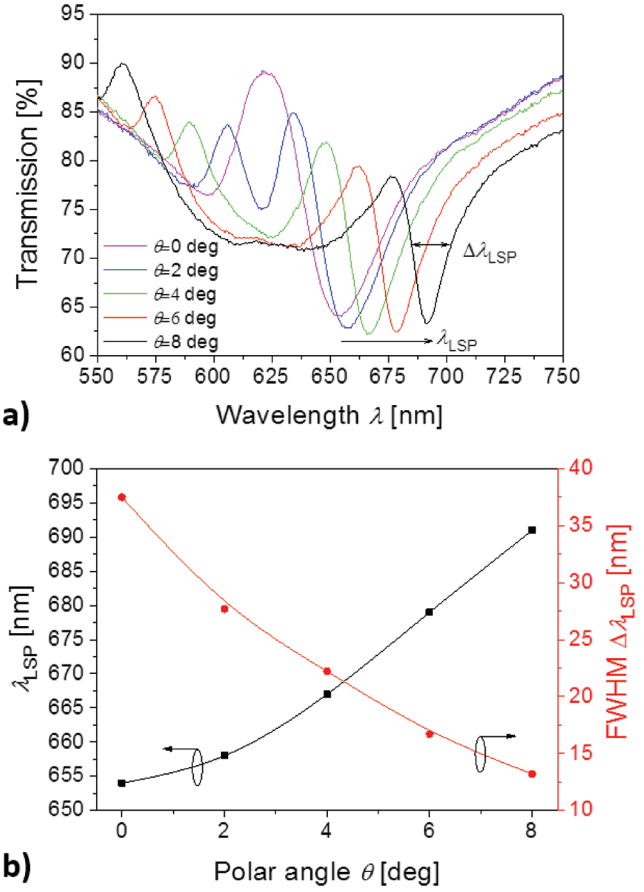

Figure 6. a) Wavelength transmission spectra measured for a tethered structure A as a function of the angle of incidence θ. The measurement was done in TE polarization at $T = 22$ °C (swollen state) for a structure with $\Lambda = 460$ nm and $D = 110$ nm. b) Dependence of LSP wavelength position λ_{LSP} and the spectral width (FWHM) $\Delta\lambda_{LSP}$ on the angle of incidence θ.

symmetrical geometry generated by using high refractive index oils,[32] which makes the structure not suitable for biosensing applications. The response to the IgG antibody coupling is about three times larger than the variations recorded (1–2 nm) for a similar plasmonic architecture supporting cLSPs in water, composed of Au nanodisks arrays prepared on top of a low refractive index fluoropolymer (Cytop, refractive index of 1.34).[44] This can be explained by the larger probing volume and higher binding capacity conferred by the 3D hydrogel polymer networks compared to that of this architecture relying on a 2D self-assembled monolayers capping the Au nanoparticles. Moreover, it is important to note that fluoropolymers (contrary to the used hydrogel) are not suitable for chemical modification and are prone to unspecific sorption from complex samples, which complicates their utilization in biosensing.

3. Conclusion

New responsive architectures enabling remarkably strong modulation of extremely spectrally narrow localized surface plasmon resonances are reported. These structures are made

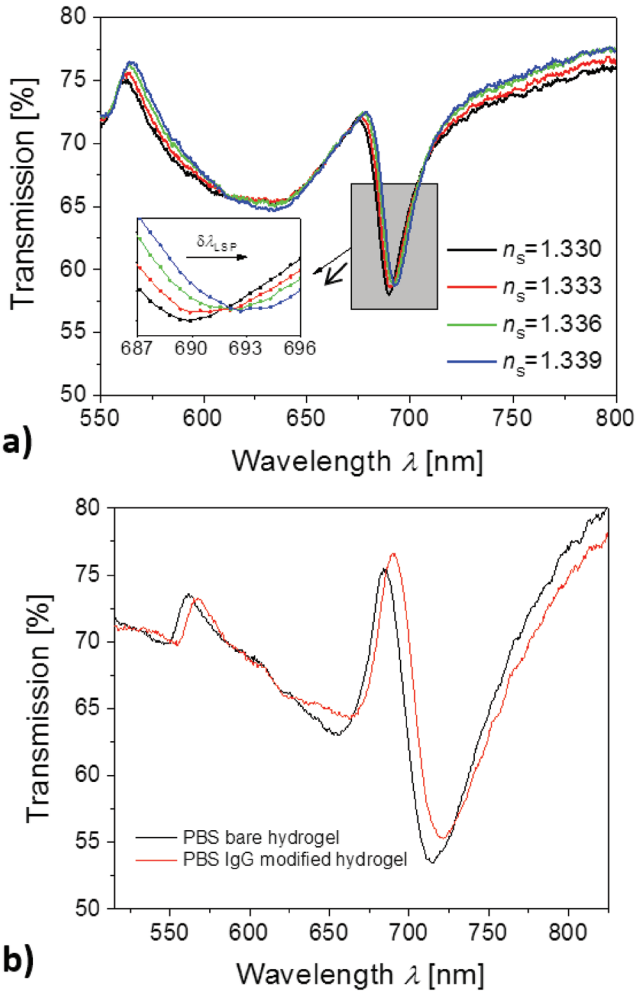

Figure 7. Measured dependence of LSP transmission spectra for tethered structure A on a) refractive index of a liquid brought in contact with the arrays of gold nanoparticles (prepared with Λ = 460 nm and D = 110 nm) and b) measured transmission changes due to the post-modification of the pNIPAAm-based polymer network with IgG biomolecules (structure prepared with Λ = 460 nm and D = 150 nm). Measurements were performed at the angle of incidence θ = 8°.

by a technique based on template stripping combined with UV laser interference lithography. It allows for the preparation of hybrid structures with arrays of plasmonic nanoparticles attached to a thermo-responsive hydrogel membrane with tunable period and surrounding refractive index. Compared to other approaches that combine self-assembly of synthetically-made spherical metallic nanoparticles and thermo-responsive polymer for actuating of hexagonal arrays with domain size <mm,[45] the reported approach offers more versatile preparation means with controlled shape of nanoparticles and lattice configurations over larger areas with characteristic size >cm, and it enables actuating of the arrays period for free-standing membrane configuration. We demonstrate that the temperature modulation or exchanging the solvent allows for reversible shifting of plasmonic resonances in the near infrared part of the spectrum by up to 150 nm, which exceeds the spectral width of the resonance as low as 13 nm and allows its complete switching "on" and "off." The potential capabilities for biosensing with the tethered configuration employing a hydrogel that can be post-modified with protein ligands are assessed for the refractometric localized surface plasmon resonance biosensors, where a figure of merit as high as 29 was observed. The plasmonic architectures with on-demand tunable optical properties also hold potential to be employed as active plasmonic substrates in other biosensor modalities taking advantage of plasmonically amplified optical spectroscopy[17,46] and in miniature machines.[47] For instance, the tunable plasmonic wavelength may find its applications in multiplexed plasmon-enhanced fluorescence sensing or for the fine-tuning of surface-enhanced Raman spectroscopy enhancement for specific vibration bands.

4. Experimental Section

Materials: Trichloro(1H,1H,2H,2H-perfluorooctyl)silane (perfluoro-silane) was obtained from Sigma-Aldrich (Germany). S1805 and A-Z303 from Microresist Technology (Germany) were employed as positive photoresist and its developer, respectively. Ostemer 322 Crystal Clear was purchased from Mercene Labs AB (Sweden). Polydimethylsiloxane Sylgard 184 was obtained from Dow Corning (USA). Dimethyl sulfoxide (DMSO), *N*-hydroxysuccinimide (NHS), *N*-(3-dimethylaminopropyl)-*N*′-ethylcarbodiimide hydrochloride (EDC), and immunoglobulin G (IgG) antibody from mouse serum were purchased from Sigma-Aldrich (Germany). Bis(acryloyl)cystamide (BAC, 98%) was from Alfa Aesar (Germany). *N*,*N*′-Methylenebis(acrylamide) (99%), 2-hydroxy-4′-(2-hydroxyethoxy)-2-methylpropiophenone (98%), and tris(2-carboxyethyl)-phosphine hydrochloride (TCEP, ≥98%) were acquired from Sigma-Aldrich (Germany). *N*-Isopropylacrylamide (97%) from Sigma-Aldrich (Germany) was recrystallized from hexane and stored under nitrogen in the fridge until needed. In addition, a pNIPAAm-based terpolymer (composed of *N*-isoproprylacrylamide, methacrylic acid, and *N*-(4-benzoylphenyl)prop-2-enamide at a ratio of 94:5:1) together with benzophenone-disulfide was synthesized as reported elsewhere.[48]

Preparation of Gold Particle Arrays: Perfluoro-silane was vapor deposited onto the surface of BK7 glass substrates. Briefly, the substrate was placed into an evacuated desiccator with the volume of 5.8 L and together with 13 µL of perfluorosilane heated to T = 250 °C for 20 min. Then, the substrate was removed and coated by a 50 nm thick gold film by vacuum evaporation (HHV AUTO 306 from HHV LTD) in vacuum better than 2×10^{-6} mbar. Afterward, the gold layer was structured in order to yield periodic arrays of plasmonic nanoparticles. First, 100 nm thick S1805 resist layer was spun on top of the gold surface, followed by the recording of a periodic pattern by UV laser interference lithography according to protocol reported before.[36] Coherent beam was emitted at a wavelength of 325 nm from a HeCd laser (IK 3031 R-C from Kimmon, Japan) and exposure time was adjusted for the recording to yield an irradiation dose of 6.75 mJ cm^{-2}. The beam was split to two interfering collimated waves with the angle between them set to 26.83°, 20.69°, and 16.87°, which translates to periodicities Λ of 360, 460, and 560 nm respectively. The pattern recorded in the photoresist layer was developed by AZ-303 developer forming periodic arrays of photoresist cylindrical features. The diameter of the photoresist features was adjusted by varying the development time between 150–240 s. Finally, the relief photoresist structure was transferred to the underneath gold layer by ion etching (450 s, 70°) with the IonSys 500 instrument from Roth & Rau (Germany). The remaining photoresist on top of the prepared gold nanoparticles was removed by an oxygen plasma treatment (5 min, 1 mbar and 40 W).

Attachment of the Gold Nanoparticles to a Tethered Hydrogel Cushion: First, the perfluoro-silane was deposited again in between the gold nanostructures on BK7 glass substrate, as described above. Afterward,

Table 1. Overview of actuating of LSP wavelength for tethered and free-standing structures and comparison of refractive index sensitivity to variations in the bulk refractive index n_s.

Geometrical parameters	$\delta\lambda_{LSP}$ [nm]	$\Delta\lambda_{LSP}$ [nm]	$\delta\lambda_{LSP}/\delta n_s$ [nm/RIU]	$\Delta\lambda_{LSP}$ [nm]	$\delta\lambda_{LSP}/\delta n_s$ [nm/RIU]
	T = 22–45 °C	Swollen T = 22 °C	Swollen T = 22 °C	Collapsed T = 45 °C	Collapsed T = 45 °C
A) Tethered hydrogel structure					
Λ = 460 nm D = 110 nm	18.5	38 (θ = 0°) 13 (θ = 8°)	373	73 (θ = 0°)	190
Λ = 460 nm D = 150 nm	28.6	88 (θ = 0°) 45 (θ = 8°)	327	75 (θ = 0°)	134
Λ = 560 nm D = 150 nm	29.5	56 (θ = 0°) 35 (θ = 8°)	475	98 (θ = 0°)	329
Λ = 560 nm D = 200 nm	28.2	135 (θ = 0°) 102 (θ = 8°)	463	96 (θ = 0°)	246
B) Free standing hydrogel structure					
Λ = 360 nm D = 140 nm	61 (H_2O) 151 (EtOH)	66 (H_2O) 22 (EtOH)	–	120	–

the substrate was incubated overnight in a 1×10^{-3} M solution of benzophenone-disulfide dissolved in DMSO in order to form a self-assembled monolayer on the gold nanoparticles. Then a 3 wt% ethanolic solution of the pNIPAAm-based terpolymer was spun at 2000 rpm for 60 s on the substrate, and dried overnight at T = 50 °C in a vacuum oven. The resulting film with a thickness of about 275 nm was crosslinked via the benzophenone moieties attached to the polymer chains by the irradiation with UV-lamp at a wavelength of 365 nm (irradiation dose of 10 J cm^{-2}). Subsequently, a drop of Ostemer resin was deposited onto the surface of another clean BK7 glass substrate and spread by pressing a flat block of PDMS on top of the droplet to form a thin layer. The Ostemer was pre-cured by irradiation with UV light at a wavelength of 365 nm (irradiation dose of 2 J cm^{-2}) through the PDMS block. Then the PDMS block was peeled-off and the substrate with the pre-cured Ostemer surface was pressed against the previously prepared gold nanoparticle arrays covered with the crosslinked pNIPAAm-based film. The elastic pre-cured Ostemer was overnight allowed to bind to the pNIPAAm-based surface via its epoxy groups at T = 50 °C. Finally, the hydrogel film with attached gold nanoparticle arrays was separated from the perfluoro-silane modified BK7 substrate, see Figure 1.

Attaching Gold Nanoparticles to Free-Standing Hydrogel Cushion: The functionalization of gold nanoparticles with a thiol-acrylates was done by the in situ generation of *N*-(2-mercaptoethyl)acrylamide through the reduction of BAC with TCEP. In a typical experiment 10.42 mg (2×10^{-3} M) of BAC and 11.47 mg (2×10^{-3} M) TCEP were added to 20 mL of ethanol, and the mixture was heated to help dissolving the solids. The gold nanoparticles arrays were incubated in the freshly prepared solution for 1 h, followed by washing with ethanol and drying with a stream of dry nitrogen. Afterward, pNIPAAm film was polymerized on the top of this surface by using 1 g *N*-isopropylacrylamide monomer, 13.6 mg *N*,*N*′-methylenebis(acrylamide) as a crosslinker and 19.8 mg 2-hydroxy-4′-(2-hydroxyethoxy)-2-methylpropiophenone as a photoinitiator dissolved in DMSO. The polymerization was made in a home-built cell with a height of about 40 µm under UV-irradiation in nitrogen environment (O_2 < 0.5%). The final structures were obtained by releasing the hydrogels by overnight incubation in ethanol yielding free-standing polymer networks with the gold particles upon drying.

Morphological Characterization: Atomic force microscopy in tapping mode was employed to study the topography of the tethered hydrogel film with arrays of gold nanoparticles. The measurements in air were performed by PicoPlus (Molecular Imaging, Agilent Technologies, USA), while the measurements in water were carried out by Nanowizard III (JPK Instruments, Germany) with temperature control by a Peltier element in the flow cell. The surfaces were probed by silicon nitride cantilevers DNP-S10 (Bruker, USA) with a nominal spring constant of 0.24 N m^{-1}. Optical microscopy observation of nanoparticle arrays was performed with a Nanopsis M instrument (Nanopsis Ltd., UK) utilizing super-resolution microsphere amplifying lens with a focal length of 1–2 µm (using a 20 µm diameter barium titanate microsphere attached to the amplifying lens).

Optical Spectroscopy of cLSPs: Transmission spectroscopy measurements were carried out using an in-house developed optical system that was described in detail before.[36,49] Briefly, a sample with arrays of gold nanoparticles was mounted on a rotation stage driven by a stepper motor from Huber GmbH (Germany), in order to control the polar angle of collimated polychromatic light beam θ impinging at its surface. The sample was interfaced with a flow-cell consisting of a thin PDMS gasket and transparent quartz substrate. The flow-cell with a volume of about 10 µL was temperature controlled by using a Peltier device[17] that was connected to a driver LFI3751 from Wavelength Electronics (USA). The spectrum of light that passed through the sample was recorded by the spectrometer HR4000 from Ocean Optics (USA) or Shamrock SR-303I-B from Andor Technology (Ireland). The data were acquired and analyzed by a home-developed software in Labview from National Instruments (USA) or the software Solis from Andor Technology (UK). The acquired transmission spectra were normalized with the reference spectrum measured without the sample and corrected for the dark signal. Transporting of liquid samples through the flow-cell was conducted via fluidic tubing Tygon and a peristaltic pump from Ismatec (Switzerland) at a flow rate of 50 µL min^{-1}. In refractometric experiments, a series of water samples were spiked with sucrose at a concentration between 2% and 6% (sucrose increases the refractive index by 1.5×10^{-3} refractive index units per %). The in situ post-modification of tethered pNIPAAm-based hydrogel was carried out incorporating IgG antibodies. The carboxylic groups carried by the crosslinked terpolymer were reacted with a mixture of EDC (75 mg mL^{-1}) and NHS (21 mg mL^{-1}) in water for 30 min. After rinsing with phosphate buffered saline (PBS), IgG protein dissolved (50 µg mL^{-1}) in acetate buffer (pH = 4) was flowed over the hydrogel surface for 60 min and finally rinsed with PBS.

Numerical Simulations: The finite difference time domain (FDTD) method that was implemented in a commercial software from Lumerical Inc. (Canada) was employed. The geometry of nanoparticle arrays was described by using Cartesian coordinates with the *x* and *y* axis in the plane and with *z* axis perpendicular to the plane of the arrays. A single unit cell with a uniform mesh size of 2 nm in all three directions was used to calculate the near field electric intensity and the far-field transmission spectra. Convergence checks lead to the conclusion that this mesh size was sufficient for accurate results. A transmission monitor was placed 0.4 µm below the nanoparticle arrays and a 2D monitor in the *xz*-plane was employed for simulating near field distribution of the electric field intensity. The perfectly matched layers (PML) above and below the

structure and periodic Bloch boundary conditions in *x*- and *y*-direction were employed. Optical constants of gold were taken from literature.[50] Refractive index of a collapsed hydrogel membrane was estimated as $n_h = 1.46$, that of the membrane swollen in water as $n_h = 1.34$ (refractive index of solvent $n_s = 1.331$ at 700 nm and $T = 25$ °C), and after swelling in ethanol as $n_h = 1.36$ (refractive index of water $n_s = 1.359$ at 700 nm and $T = 20$ °C). These values were obtained assuming the volumetric swelling ratio in water of 8 (same material showed swelling in each direction of about 2 as observed for micro-disks[17,46]) and by relating this swelling ratio to data measured for similar thin hydrogel films with same volume swelling ratio.[17]

Acknowledgements

N.G.Q., M.v.D., and D.K. acknowledge funding from the European Union's Horizon 2020 research and innovation programme under grant agreement No 642787, Marie Sklodowska-Curie Innovative Training Network BIOGEL, P.V. from the project jointly funded by Agence Nationale de la Recherche (ANR) and Austrian Science Fund (FWF) under the grant agreements ANR-15-CE29-0026 and I 2647, respectively. C.P. received support from the European Union's Horizon 2020 research and the innovation program under Grant Agreement No. 633937, project ULTRAPLACAD.

Conflict of Interest

The authors declare no conflict of interest.

Keywords

active plasmonics, biosensing, lattice resonance, metallic nanoparticles, responsive hydrogels

Received: February 26, 2019
Revised: April 19, 2019
Published online: May 20, 2019

[1] D. K. Gramotnev, S. I. Bozhevolnyi, *Nat. Photonics* **2010**, *4*, 83.
[2] a) J. A. Schuller, E. S. Barnard, W. Cai, Y. C. Jun, J. S. White, M. L. Brongersma, *Nat. Mater.* **2010**, *9*, 193; b) E. Ozbay, *Science* **2006**, *311*, 189.
[3] a) H. A. Atwater, A. Polman, *Nat. Mater.* **2010**, *9*, 205; b) A. Aubry, D. Y. Lei, A. I. Fernández-Domínguez, Y. Sonnefraud, S. A. Maier, J. B. Pendry, *Nano Lett.* **2010**, *10*, 2574.
[4] a) P. Wang, B. Huang, Y. Dai, M.-H. Whangbo, *Phys. Chem. Chem. Phys.* **2012**, *14*, 9813; b) I. Thomann, B. A. Pinaud, Z. Chen, B. M. Clemens, T. F. Jaramillo, M. L. Brongersma, *Nano Lett.* **2011**, *11*, 3440.
[5] a) H. Wei, H. Xu, *Nanophotonics* **2012**, *1*, 155; b) Y. Fang, M. Sun, *Light: Sci. Appl.* **2015**, *4*, e294.
[6] A. J. Haes, C. L. Haynes, A. D. McFarland, G. C. Schatz, R. P. Van Duyne, S. Zou, *MRS Bull.* **2005**, *30*, 368.
[7] a) B. Špačková, P. Wrobel, M. Bocková, J. Homola, *Proc. IEEE* **2016**, *104*, 2380; b) M. E. Stewart, C. R. Anderton, L. B. Thompson, J. Maria, S. K. Gray, J. A. Rogers, R. G. Nuzzo, *Chem. Rev.* **2008**, *108*, 494.
[8] S. Lal, N. K. Grady, J. Kundu, C. S. Levin, J. B. Lassiter, N. J. Halas, *Chem. Soc. Rev.* **2008**, *37*, 898.
[9] a) K. F. MacDonald, Z. L. Sámson, M. I. Stockman, N. I. Zheludev, *Nat. Photonics* **2009**, *3*, 55; b) L. Cao, M. L. Brongersma, *Nat. Photonics* **2009**, *3*, 12; c) K. F. MacDonald, N. I. Zheludev, *Laser Photonics Rev.* **2010**, *4*, 562; d) B. Gjonaj, J. Aulbach, P. M. Johnson, A. P. Mosk, L. Kuipers, A. Lagendijk, *Nat. Photonics* **2011**, *5*, 360.
[10] a) A. Emboras, C. Hoessbacher, C. Haffner, W. Heni, U. Koch, P. Ma, Y. Fedoryshyn, J. Niegemann, C. Hafner, J. Leuthold, *IEEE J. Sel. Top. Quantum Electron.* **2015**, *21*, 276; b) W. Cai, J. S. White, M. L. Brongersma, *Nano Lett.* **2009**, *9*, 4403.
[11] a) V. K. Hsiao, Y. B. Zheng, B. K. Juluri, T. J. Huang, *Adv. Mater.* **2008**, *20*, 3528; b) T. Ming, L. Zhao, M. Xiao, J. Wang, *Small* **2010**, *6*, 2514.
[12] a) T. Ellenbogen, K. Seo, K. B. Crozier, *Nano Lett.* **2012**, *12*, 1026; b) L. Wang, T. Li, R. Guo, W. Xia, X. Xu, S. Zhu, *Sci. Rep.* **2013**, *2603*, 3.
[13] a) N. Dean, *Nat. Nanotechnol.* **2015**, *10*, 15; b) Z. Li, A. W. Clark, J. M. Cooper, *ACS Nano* **2016**, *10*, 498; c) K. Xiong, D. Tordera, G. Emilsson, O. Olsson, U. Linderhed, M. P. Jonsson, A. B. Dahlin, *Nano Lett.* **2017**, *17*, 7033.
[14] a) M. G. Manera, E. Ferreiro-Vila, J. M. Garcia-Martin, A. Garcia-Martin, R. Rella, *Biosens. Bioelectron.* **2014**, *58*, 114; b) Y. B. Zheng, Y.-W. Yang, L. Jensen, L. Fang, B. K. Juluri, A. H. Flood, P. S. Weiss, J. F. Stoddart, T. J. Huang, *Nano Lett.* **2009**, *9*, 819; c) D. Yoo, T. W. Johnson, S. Cherukulappurath, D. J. Norris, S.-H. Oh, *ACS Nano* **2015**, *9*, 10647.
[15] N. Jiang, X. Zhuo, J. Wang, *Chem. Rev.* **2018**, *118*, 3054.
[16] a) G. K. Joshi, K. N. Blodgett, B. B. Muhoberac, M. A. Johnson, K. A. Smith, R. Sardar, *Nano Lett.* **2014**, *14*, 532; b) J. Dintinger, I. Robel, P. V. Kamat, C. Genet, T. W. Ebbesen, *Adv. Mater.* **2006**, *18*, 1645.
[17] M. Toma, U. Jonas, A. Mateescu, W. Knoll, J. Dostalek, *J. Phys. Chem. C* **2013**, *117*, 11705.
[18] J.-W. Jeon, J. Zhou, J. A. Geldmeier, J. F. Ponder Jr., M. A. Mahmoud, M. El-Sayed, J. R. Reynolds, V. V. Tsukruk, *Chem. Mater.* **2016**, *28*, 7551.
[19] V. Stockhausen, P. Martin, J. Ghilane, Y. Leroux, H. Randriamahazaka, J. Grand, N. Felidj, J. C. Lacroix, *J. Am. Chem. Soc.* **2010**, *132*, 10224.
[20] a) W. Lu, N. Jiang, J. Wang, *Adv. Mater.* **2017**, *29*, 1604862; b) N. Jiang, L. Shao, J. Wang, *Adv. Mater.* **2014**, *26*, 3282.
[21] Z. Sun, W. Ni, Z. Yang, X. Kou, L. Li, J. Wang, *Small* **2008**, *4*, 1287.
[22] I. Tokareva, S. Minko, J. H. Fendler, E. Hutter, *J. Am. Chem. Soc.* **2004**, *126*, 15950.
[23] M. L. Tseng, J. Yang, M. Semmlinger, C. Zhang, P. Nordlander, N. J. Halas, *Nano Lett.* **2017**, *17*, 6034.
[24] a) Y. Yao, M. A. Kats, P. Genevet, N. Yu, Y. Song, J. Kong, F. Capasso, *Nano Lett.* **2013**, *13*, 1257; b) Y. Yao, M. A. Kats, R. Shankar, Y. Song, J. Kong, M. Loncar, F. Capasso, *Nano Lett.* **2014**, *14*, 214.
[25] G. Lilley, M. Messner, K. Unterrainer, *Opt. Mater. Express* **2015**, *5*, 2112.
[26] Y. Chu, E. Schonbrun, T. Yang, K. B. Crozier, *Appl. Phys. Lett.* **2008**, *93*, 181108.
[27] S. R. K. Rodriguez, A. Abass, B. Maes, O. T. Janssen, G. Vecchi, J. G. Rivas, *Phys. Rev. X* **2011**, *1*, 021019.
[28] M. Bauch, J. Dostalek, *Opt. Express* **2013**, *21*, 20470.
[29] a) B. Ng, S. Hanham, V. Giannini, Z. Chen, M. Tang, Y. Liew, N. Klein, M. Hong, S. Maier, *Opt. Express* **2011**, *19*, 14653; b) P. Offermans, M. C. Schaafsma, S. R. Rodriguez, Y. Zhang, M. Crego-Calama, S. H. Brongersma, J. Gómez Rivas, *ACS Nano* **2011**, *5*, 5151.
[30] a) K. Carron, W. Fluhr, M. Meier, A. Wokaun, H. Lehmann, *J. Opt. Soc. Am. B* **1986**, *3*, 430; b) G. Vecchi, V. Giannini, J. G. Rivas, *Phys. Rev. Lett.* **2009**, *102*, 146807.
[31] Z. Li, S. Butun, K. Aydin, *ACS Nano* **2014**, *8*, 8242.
[32] W. Zhou, M. Dridi, J. Y. Suh, C. H. Kim, M. R. Wasielewski, G. C. Schatz, T. W. Odom, *Nat. Nanotechnol.* **2013**, *8*, 506.
[33] a) B. Auguié, W. L. Barnes, *Phys. Rev. Lett.* **2008**, *101*, 143902; b) A. D. Humphrey, W. L. Barnes, *Phys. Rev. B* **2014**, *90*, 075404.

[34] J. Q. Li, J. Ye, C. Chen, L. Hermans, N. Verellen, J. Ryken, H. Jans, W. Van Roy, V. V. Moshchalkov, L. Lagae, P. Van Dorpe, *Adv. Opt. Mater.* **2015**, *3*, 176.
[35] K. Volk, J. P. Fitzgerald, P. Ruckdeschel, M. Retsch, T. A. König, M. Karg, *Adv. Opt. Mater.* **2017**, *5*, 1600971.
[36] N. G. Quilis, M. Lequeux, P. Venugopalan, I. Khan, W. Knoll, S. Boujday, M. L. de la Chapelle, J. Dostalek, *Nanoscale* **2018**, *10*, 10268.
[37] M. J. Junk, R. d. Berger, U. Jonas, *Langmuir* **2010**, *26*, 7262.
[38] Y. Wang, C.-J. Huang, U. Jonas, T. Wei, J. Dostalek, W. Knoll, *Biosens. Bioelectron.* **2010**, *25*, 1663.
[39] B. Špačková, J. Homola, *Opt. Express* **2013**, *21*, 27490.
[40] I. Anac, A. Aulasevich, M. J. N. Junk, P. Jakubowicz, R. F. Roskamp, B. Menges, U. Jonas, W. Knoll, *Macromol. Chem. Phys.* **2010**, *211*, 1018.
[41] Q. Zhang, Y. Wang, A. Mateescu, K. Sergelen, A. Kibrom, U. Jonas, T. Wei, J. Dostalek, *Talanta* **2013**, *104*, 149.
[42] C. J. Huang, J. Dostalek, W. Knoll, *Biosens. Bioelectron.* **2010**, *26*, 1425.
[43] A. Aulasevich, R. F. Roskamp, U. Jonas, B. Menges, J. Dostalek, W. Knoll, *Macromol. Rapid Commun.* **2009**, *30*, 872.
[44] J. Li, J. Ye, C. Chen, L. Hermans, N. Verellen, J. Ryken, H. Jans, W. Van Roy, V. V. Moshchalkov, L. Lagae, *Adv. Opt. Mater.* **2015**, *3*, 176.
[45] a) K. Volk, J. P. S. Fitzgerald, P. Ruckdeschel, M. Retsch, T. A. F. Konig, M. Karg, *Adv. Opt. Mater.* **2017**, *5*, 1600971; b) K. Volk, J. P. S. Fitzgerald, M. Retsch, M. Karg, *Adv. Mater.* **2015**, *27*, 7332.
[46] M. Nguyen, I. Kherbouche, M. Braik, A. Belkhir, L. Boubekeur-Lecaque, J. Aubard, C. Mangeney, N. Felidj, *ACS Omega* **2019**, *4*, 1144.
[47] A. Mourran, H. Zhang, R. Vinokur, M. Moller, *Adv. Mater.* **2017**, *29*, 1604825.
[48] K. Sergelen, C. Petri, U. Jonas, J. Dostalek, *Biointerphases* **2017**, *12*, 051002.
[49] I. Khan, H. Keshmiri, F. Kolb, T. Dimopoulos, E. J. List-Kratochvil, J. Dostalek, *Adv. Opt. Mater.* **2016**, *4*, 435.
[50] P. B. Johnson, R.-W. Christy, *Phys. Rev. B* **1972**, *6*, 4370.

